CrossMark

Influences of Post-processing, Location, Orientation, and Induced Porosity on the Dynamic Compression Behavior of Ti–6Al–4V Alloy Built Through Additive Manufacturing

S. Gangireddy[1] · E. J. Faierson[2] · R. S. Mishra[1]

Abstract

This paper investigates the dynamic compression behavior of Ti–6Al–4V alloy built through powder bed fusion (PBF) additive manufacturing. Samples of 45 different conditions were examined: Builds of three different orientations (vertical, horizontal, and 45° tilt), built in five different locations around the build plate (four corners and center), in as-built, stress-relieved and hot isostatically pressed conditions. High strain rate behavior was evaluated using a Split-Hopkinson Pressure Bar testing system. The as-built builds showed significant scatter with respect to both orientation and location owing to high internal stresses. Stress relief treatment resulted in a locationally uniform response but the retained columnar structure gave rise to higher strength in 45° tilt builds, along with a higher propensity for failure by shear localization. Hot isostatic pressing was found to be a necessary treatment for a truly homogeneous response that was independent of orientation and location on the build plate. A second series of samples were built in porous sandwich form with modification of processing parameters in the core to produce varying amounts of porosity. Porous samples exhibited greater energy absorption per unit volume than fully dense samples. Largest energy absorption capacity was observed in the samples with minimal porosity due to delayed failure without a significant loss in strength.

Introduction

Additive manufacturing (AM) is a rapidly growing technology that enables components to be built in layers by adding material to the previous layer. Two types of metal additive manufacturing technology are direct energy deposition (DED) and powder bed fusion (PBF). In the DED process, metal powder is sprayed through nozzles into a laser beam, where it is melted and deposited onto a surface. PBF process is a type of additive manufacturing in which metal powder is spread across an area using a recoating mechanism. Each layer of metal powder deposited is then be melted using a heat source such as a laser [1]. The powder bed fusion process can be used to build a variety of complex geometries, such as internal channels, which cannot be fabricated using conventional subtractive machining technology. AM is especially attractive in high value commercial alloys like Ti–6Al–4V with machining problems. Ti–6Al–4V has relatively low density and good strength enabling utilization in a number of industries including aerospace and defense [2] and can be readily used in the PBF process to fabricate components.

However, microstructural development is highly dependent on the temperature regime of heat treatment for Ti–6Al–4V produced through PBF processes [1–3]. Ti–6Al–4V is well documented to produce heterogeneous structures with columnar prior-β grain morphology and grain boundary alpha phase which leads to anisotropy in the mechanical response [4, 5]. While it has been shown that microstructural and quasi-static mechanical properties can vary across regions of a component [6], literature on dynamic response has been limited.

Split-Hopkinson Pressure Bar (SHPB) testing is a method to evaluate high strain rate performance. A few prior studies

✉ S. Gangireddy
sindhu.g.reddy@gmail.com

1   Advanced Materials and Manufacturing Processes Institute, University of North Texas, Denton, TX, USA

2   Quad City Manufacturing Lab, Western Illinois University, Macomb, IL, USA

have examined high strain rate performance of commercial hot-rolled Ti–6Al–4V and specimens fabricated by DED. While the hot-rolled Ti–6Al–4V bars showed yield strength of 998 and 1010 MPa at room temperature under strain rates of 800 and 1400 s^{-1}, respectively [7], the DED specimens showed higher strengths of ~ 1350 MPa at 10% strain under a strain rate of 1000 s^{-1} [8]. The latter study also explored porosity effect of 10% and 20% porous samples which showed flow stresses of 1350, and 1200 MPa respectively at 10% strain. So unlike the quasi-static properties, the dynamic response of the heterogeneous AM Ti–6Al–4V alloy has not been well explored. In this study we conduct a comprehensive investigation using 45 different conditions. Cylindrical specimens were built using standard settings at five different locations on the build plate (four corners and at center) in three different orientations (cylindrical specimen axial direction at 0°, 90°, and 45° to the build plate). Two sets of these cylinders were subjected to post-processing heat treatments, stress relief and hot-isostatic press (HIP). We explore both the effects of post-build heat treatments on the dynamic mechanical response of Ti–6Al–4V alloy built through PBF, while simultaneously studying the anisotropy due to columnar microstructures of additive materials by varying build orientation, and the uniformity of the properties at various locations on the build plate.

In a second series of experiments, porous sandwich specimens were fabricated through process parameter modification and had varying amounts of induced porosity in their core. A previous study investigated Super Alloy 718 built using the PBF process and modified process conditions including laser power, scan speed, and hatch spacing to induce various levels of porosity within specimens [9]. Porosity has also been generated in titanium using a powder bed fusion process that mimics the structure of human bone [10]. Uniaxial compression tests were performed using SHPB on all these specimens. Optical and electron microscopes were used to characterize the initial microstructures in the three conditions as well as the fractured surfaces with

deformation features in the specimens that have undergone shear failure. Correlation of dynamic flow stresses and their fracture strains to the microstructural observations is highlighted.

Experimental Procedure

Material

Ti–6Al–4V SHPB samples with dimensions of 5 mm diameter and 5 mm height were built on an EOS M270 PBF system. Ti–6Al–4V powder was sourced from Advanced Powders and Coatings (APC) with a particle size ranging from 15 to 45 μm. Three builds of Ti–6Al–4V Split-Hopkinson Pressure Bar (SHPB) specimens were created, with thirty specimens fabricated in each build. The specimens were built in five different zones on the build plate, rear left (X), rear right (V), front left (O), front right (D), and center (C) as shown in Fig. 1. Six specimens were fabricated in each zone. Two specimens were fabricated in each orientation, vertical, horizontal, and 45° within each zone. Due to their orientations, the horizontal and 45° specimens required support structure. The specimens were built with a laser power of 170 W, scan speed of 1250 mm s^{-1}, hatch spacing of 0.1 mm, and layer thickness of 0.03 mm. These standard settings are designed for fully dense builds. After each build, the specimens were removed from the build plate using a wire EDM.

The specimens on the first build were tested in as-built condition. The specimens on the second build were stress relieved at 650 °C for 3 h in an argon atmosphere before removal from the build plate. The specimens on the third build were stress relieved using the parameters above, removed from the build plate, and then hot isostatic pressed (HIP) at 1000 °C and 14,500 psi for 2 h in an argon atmosphere, followed by a cooling rate of 17 °C min^{-1}. Subjecting the builds to both high temperature and isostatic gas pressure leads to reduction

Fig. 1 a Image of Ti–6Al–4V SHPB specimens after build, **b** close-up view of different orientations built in each location (inset: schematic of the three orientation builds)
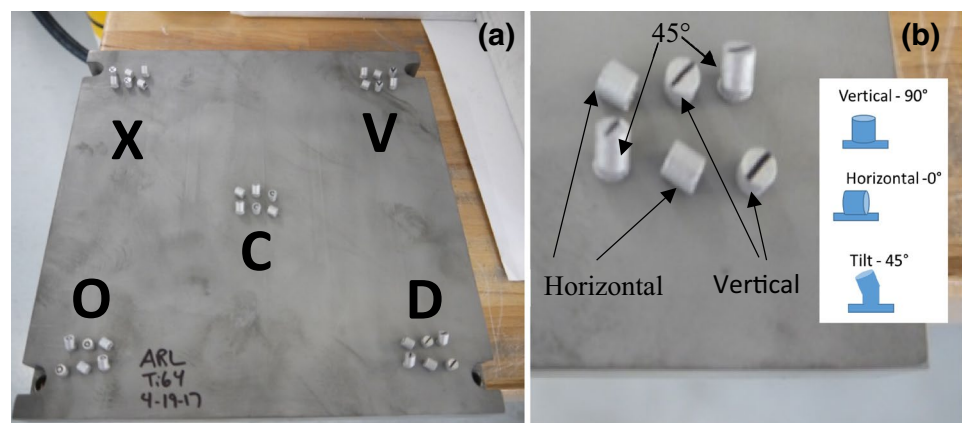
of porosity and modification of microstructure to improve mechanical properties and workability.

A separate set of cylindrical sandwich specimens were built with 1.5 mm of face plates which were made with the standard parameters (used in the previous builds), and 2 mm of porous cores which were made with different combinations of varying laser power, scan speed, and hatch spacing (Fig. 2). All the porous sandwiches were built in the vertical direction, perpendicular to the base plate.

SHPB Testing

Dynamic compression tests were conducted on these cylindrical specimens at a strain rate of 1500 s^{-1} on the 45 different conditions (described in the previous section) using an SHPB system. The incident, reflected and transmitted waves were analyzed according to one dimensional elastic wave theory to obtain the stress, strain rate and strain [11].

$$\sigma\,(t) = \frac{A_B\,E\,\varepsilon_t(t)}{A_S}$$

$$\dot{\varepsilon}\,(t) = \frac{2\,c_o\,\varepsilon_r(t)}{l_S}$$

$$\varepsilon\,(t) = \int_{t_i}^{t_f} \dot{\varepsilon}\,(t)\,dt\,.$$

where A_B is the cross-sectional area of the Bar, A_S and l_S are sample cross-sectional area and length respectively, E and c_o are the elastic modulus and elastic wave speed of the Bar, ε_t and ε_r are the transmitted and reflecte wave strains.

Results and Discussion

Microstructures

The as-built and stress relieved microstructures were very similar, fully dense with no visible porosity or defects. Both dplayed a martensitic microstructure composed of acicular needles (Fig. 3a, b), typical in laser AM owing to rapid heating and cooling cycles. EDS mapping showed no elemental segregation indicating a diffusionless transformation (Fig. 3c).

For a perspective on the overall structure of the builds, low magnification optical images were also studied (Fig. 4). These showed circular faceted grains of ~50 μm diameter from the top view and long columnar grains from the side view. From this, it is ascertained that the builds were composed of long columnar prior-β grains oriented along the build direction, traversing the build layers a structure typical of Ti–6Al–4V built by selective laser melting (SLM) technique. As thin layers of atomized metal powder are melted through rastering laser beam one layer after another causing rapid heating and cooling cycles, the heat flow is directed towards the build plate forming columnar microstructures.

The set of builds subjected to HIP showed a bimodal microstructure composed of basket-weave/lamellar α/β along with equiaxed α as seen in the optical image of Fig. 5a. EDS mapping confirmed the globules and the lamellae to be α, rich in Al, leaving behind a vanadium rich β matrix, Fig. 5b, which is a minor phase at RT. The diameter of the globular α grains is much larger than the width of the lamellae, so it is cleared that these regions were not cross-sections of the lamellae from a different view. The temperature of HIP treatment was above β-transus, at 1100 °C and the duration of 2 h would be sufficient for full transformation of martensitic α' into β, after which cooling at a rate of 17 °C min^{-1} normally results in a widmanstatten structure [12]. But the application of pressure during our cooling step appears to

Fig. 2 Process parameters used to generate porosity in the cores of sandwich specimens of Ti–6Al–4V

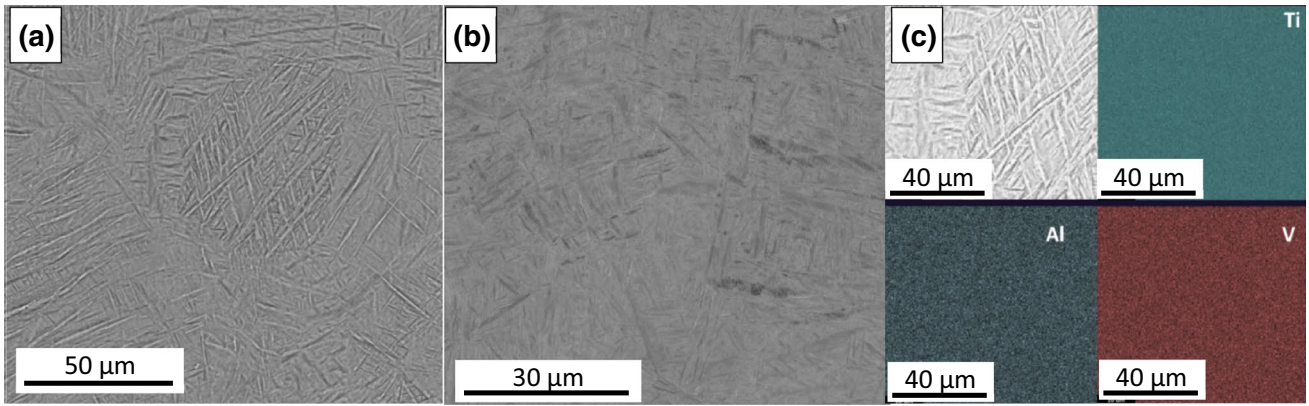|	Laser Power (W)	Scan Speed (mm/s)	Hatch Spacing (mm)	Layer Thickness (mm)
Standard	170	1250	0.10	0.03
A	170	2000	0.17	0.03
B	110	1000	0.10	0.03
C	170	1000	0.24	0.03
D	110	1000	0.24	0.03
E	170	1500	0.24	0.03
F	170	2000	0.24	0.03
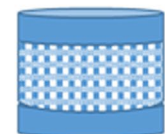
1.5mm face plates, 2mm porous core, diameter 5mm

Fig. 3 Martensitic structure of as-built and stress-relieved conditions. **a** Back scattered electron images of as-built condition—view from the top of the build, **b** back scattered electron image of the stress-relieved material, and **c** EDS map of as-built material showing no segregation in the alloying elements
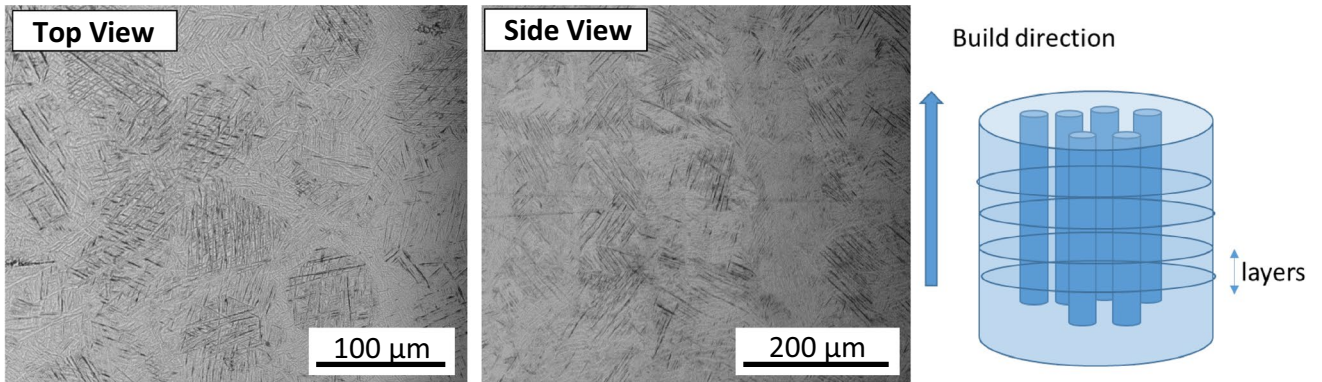

Fig. 4 Optical images from top and side views of the builds showing circular faceted grains and columnar grains, respectively. (Right) Schematic of the microstructural formation in the builds
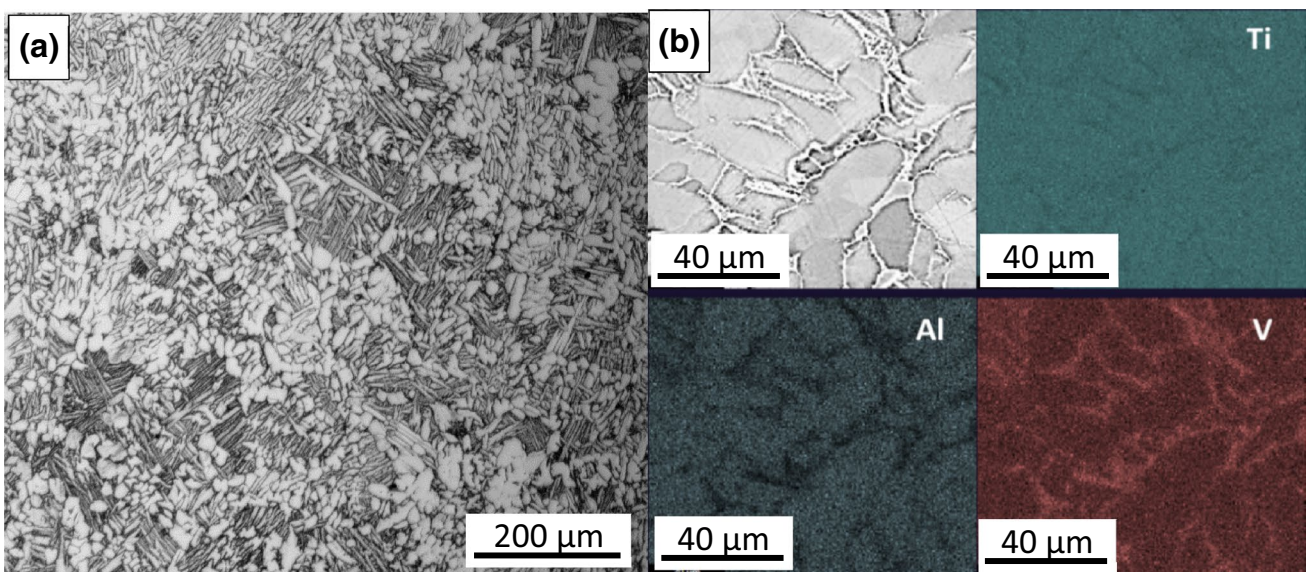

Fig. 5 **a** Optical image of the bimodal microstructure of HIP material, **b** EDS map showing Al segregation into α and high V remnant in β

have caused some partial globularization [13], resulting in this bimodal microstructure. Bimodal Ti–6Al–4V structures generally show superior mechanical properties than lamellar structures, including higher strength and better dynamic shear strength and fracture strains [14], and ultra-high cycle fatigue properties [15] and hence more desirable. Besides, favoring dynamic globularization kinetics, the high temperature in our HIP treatment also helped remove the anisotropic nature of the builds. In our HIP material, the columnar structure is largely eliminated, unlike studies such as Lu [16] who performed HIP at 920 °C for 2 h after which the columnar anisotropy in the as-built microstructure was mostly retained.

In the porous sandwiches, built by settings A–F (Fig. 2), the induced porosity in the cores was calculated through an analysis of the micrographs using ImageJ software. Figure 6 shows the wide range of porosities generated. Simultaneous reduction of both laser power and hatch spacing of yielded an almost dense specimen with disconnected minute rounded pores with a total porosity of ~2% by setting B. The other specimens showed interconnected pores and significantly higher porosity of up to 45% in the setting F with increased scanning speed coupled with increased hatch spacing.

The selective combination of process parameters across the settings A–F made it is possible to derive correlations between the individual build parameters and the final porosity and hence control over the induced porosity. Figure 7 demonstrates the porosity growing with increasing scan speed and hatch speed, but decreasing with higher laser power.

Dynamic Compression Strength

Fully Dense Builds

The results from SHPB compression tests on the fully dense specimens of three treatment conditions are summarized in Fig. 8, with each image depicting the response from across the five locations: rear left (X), rear right (V), front left (O), front right (D), and center (C). Figure 8 depicts the dynamic response from the three sets of as-built, stress-relieved and HIP'ped conditions in each of the three build orientations.

The uniformity across the locations was generally high and the stress–strain curves overlapped for the large portion. The work hardening was very small at these high strain rates of 1100 s^{-1}, typical of Ti–6Al–4V alloy. In
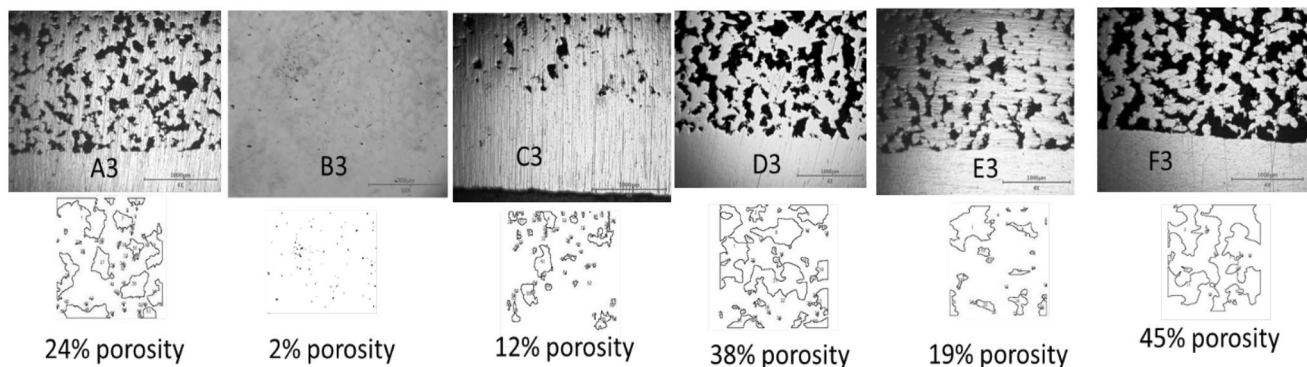

Fig. 6 Induced porosity in the cores of the sandwiches built by variation of laser power, hatch spacing, and scan speeds in settings A–F
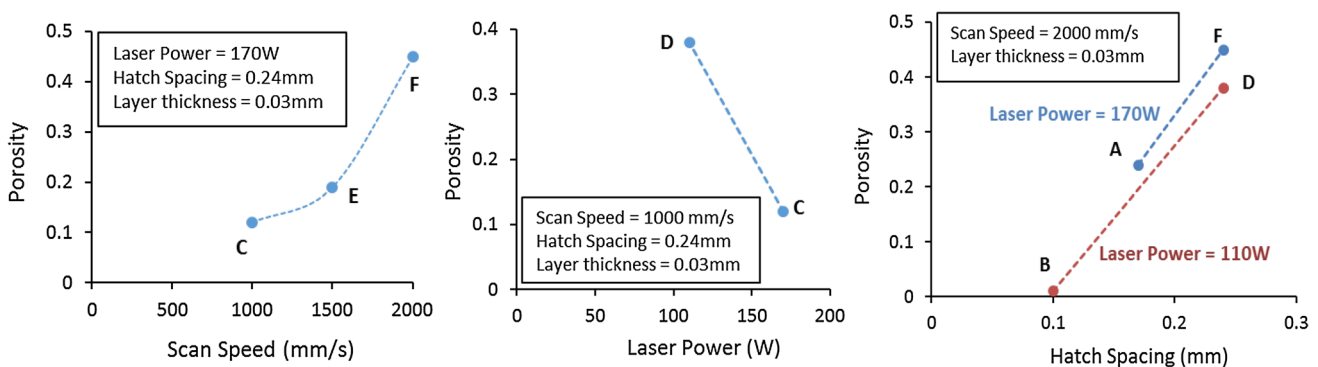

Fig. 7 Correlation of scan speed, laser power, and hatch spacing to the resultant porosity
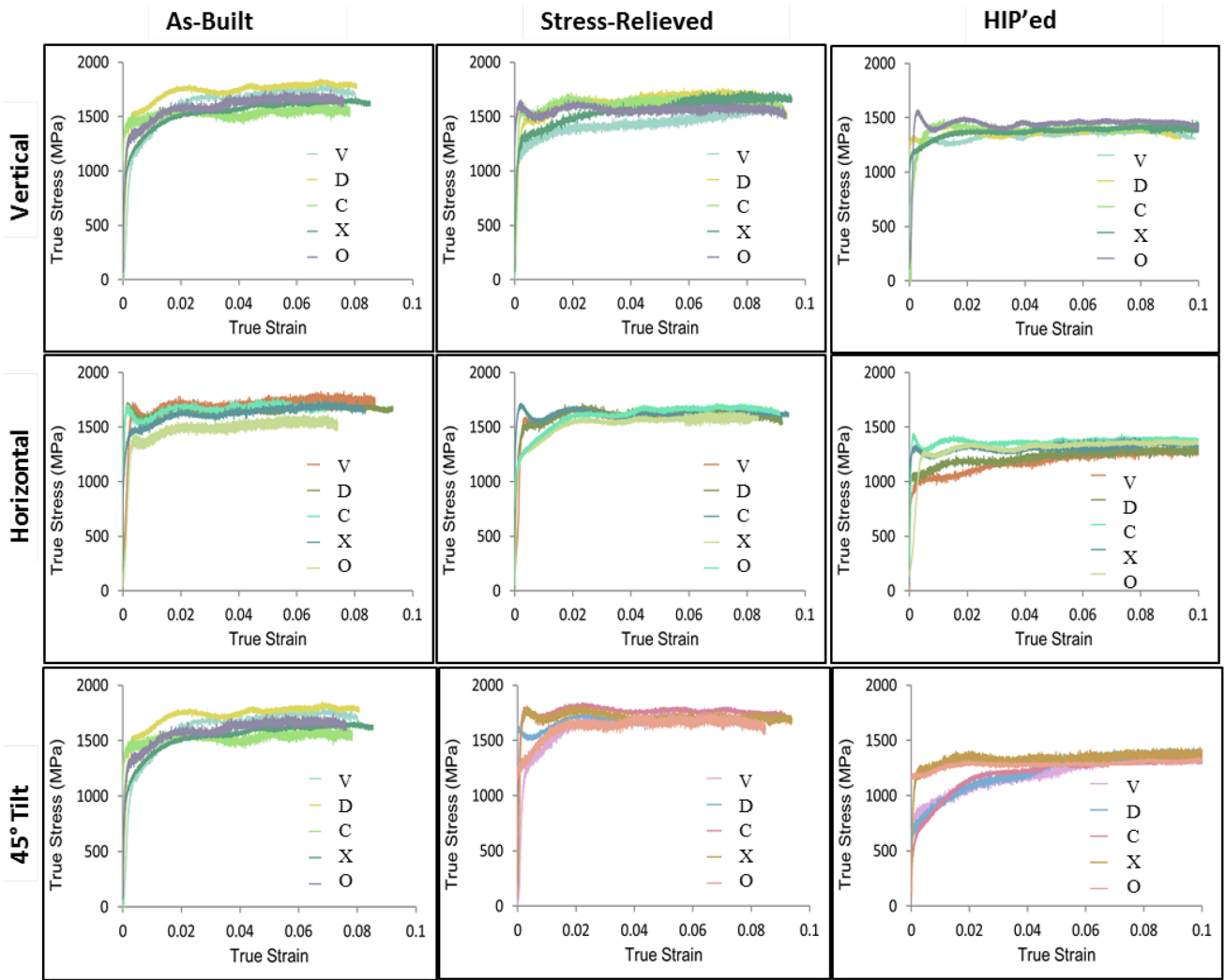
Fig. 8 Dynamic true stress–true strain curves of the five locations in: (left) as built material, (middle) stress-relieved material, and (right) HIP material. The three orientations are arranged as: (top) vertical, (middle) horizontal, and (bottom) 45°-tilt builds
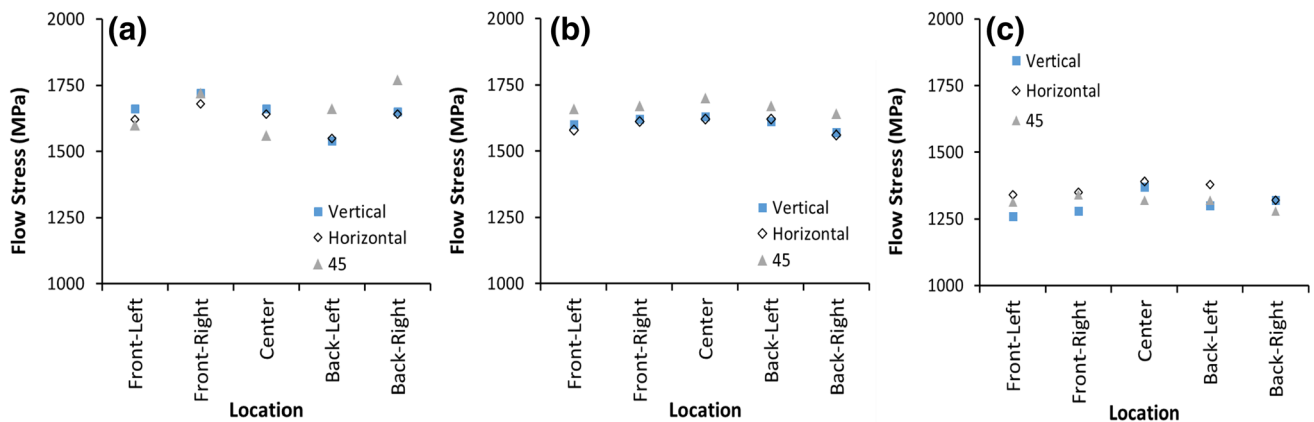

Fig. 9 Dynamic flow stress at 6% strain in **a** as-built, **b** stress-relieved, and **c** HIP conditions

order to understand the trends in this data, flow stresses at a fixed strain of 6% are compared in Fig. 9.

Figure 9 shows that both the as-built material and the stress-relieved material showed very high strengths of about 1600–1700 MPa due to their martensitic microstructure. Commercial Ti–6Al–4V alloy with 10 μm equi-axed grains has been shown to have a flow stress of about 1300–1450 MPa at room temperature under similar high strain rate deformation at 1000 s^{-1} [17, 18]. As the additive material has martensitic structure of much finer microstructure, the higher flow stresses are therefore expected. Studies on other AM materials such as 316L SS are also reported to show significantly higher strength than wrought alloys. The quasi-static YS was shown to increase from 300 to 500 MPa while dyamic flow stresses increased from 500 to 700 MPa [19].

There was a perceptible scatter in the strength across the different locations in the as-built data, with no trend with respect to orientation. The scatter was significantly mitigated in the stress-relieved data, indicating that the as-built specimens had varying magnitude of internal stresses [20]. During the repeated heating and cooling cycles, the heat flow through the base plate could have been different at the different locations [4]. Stress relief treatment which reduces the extent of internal stresses has resulted in a more *spatially* uniform data which also brings forth a clear trend with respect to orientation. The vertical builds, which have the loading axis in SHPB parallel to alignment direction of the columnar grains, appeared to have very similar dynamic flow stresses in compression as the horizontal builds where the SHPB axis is perpendicular to the grain lengths. Due to the very refined randomly oriented needles in the martensitic microstructure, there would be numerous slip planes available in any direction in these builds. So during the uniaxial compression, the dislocation motion driven by the shear stresses acting along the 45° plane would encounter maximum number of obstacles while moving perpendicular to the columnar prior-β grains (Fig. 10). Hence, it was the 45° builds that have slightly higher strength than the other two orientations. So while locational uniformity in the dynamic response could be
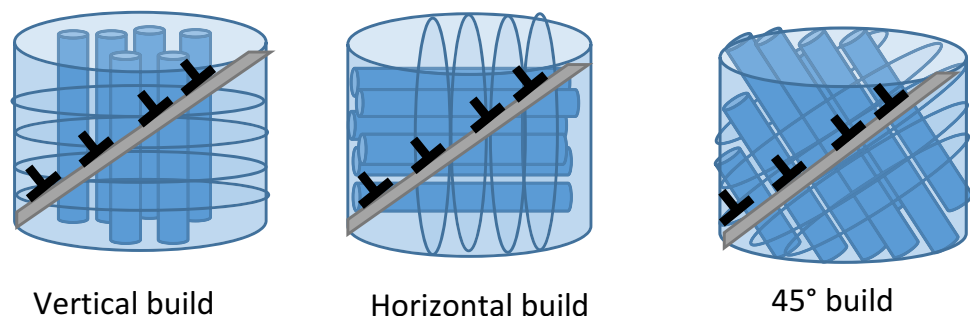
achieved by stress-relief treatment, orientation related anisotropy was present.

The HIP material, on the other hand, showed significantly lower strengths than the other two conditions at about 1400 MPa, comparable to that of the equiaxed commercial Ti–6Al–4V reported in literature [7, 21]. This was attributed to the phase transformation during HIP treatment at post β-transus temperature where martensite was converted into the bimodal α/β structure (Fig. 5). The columnar structure was also removed after the HIP treatment, and as result the flow stresses no longer show orientational anisotropy.

The martensitic microstructure in the as-built and the stress-relieved structures which made them very strong, however, also lowered their ductility. Several of the as built and stress relieved builds underwent shear failure at a mere 10%. There is once again a clear orientation influence in this anisotropic microstructure: the 45° builds have all failed, Fig. 11. This preferential failure in the 45° builds may be explained by the alignment of the maximum shear stress direction parallel to orientation of the build layers. Any defects at these layer–layer interfaces, assisted by the high strength of the martensitic structure, can result in strong stress concentrations that can trigger strain localization resulting in failure. Recent studies have revelead that dynamic properties show more anisotropy than quasistatic response in AM Ti64. Spall strength of SLM built Ti–6Al–4V showed drastic drop when tensile load was normal to the layer-interfaces due to weakness of these boundaries facilitating ready void nucleation, but tensile load along the interfaces had retained most of spall strength [22].

Figure 12 shows such a fractured surface of a 45° build after failure demonstrating presence of adiabatic shear bands. Unlike the shear bands in conventional α/β structured titanium alloys, where heat-affected zone and flow in the transition region are clearly visible [23], shear bands in this martensitic structure were significantly different. The boundary between the band and the surrounding material was sharp and there was no trace of α′ inside it. The second band in the middle of Fig. 12a appeared to be a secondary shear band in Stage 3 [24], very narrow with a width <3 μm, but had propagated across several prior-β grains

Fig. 10 Schematic showing the orientation of the columnar prior-β grains in the vertical, horizontal and 45° builds and their relative position to the shear plane

Vertical build   Horizontal build   45° build

	Horizontal	Vertical	45° Tilt
Front-Left	No Fail ε_f= 10%	Fail ε_f= 9%	Fail ε_f= 9%
Front-Right	No Fail ε_f= 10%	Fail ε_f= 10%	Fail ε_f= 10%
Center	No Fail ε_f= 10%	No Fail ε_f= 10%	Fail ε_f= 12%
Back-Left	No Fail ε_f= 11%	No Fail ε_f= 11%	Fail ε_f= 11%
Back-Right	No Fail ε_f= 10%	No Fail ε_f= 10%	Fail ε_f= 9%
Front-Left	10%	9%	9%

Fig. 11 Table highlighting the orientation dependence of the failure. Below are the pictures of the post-test specimens from the front-left location (O)

with a length of several 100 μm. The shear band on the top was further advanced with an increased width of almost 10 μm and was developing into a primary shear zone. The former band was also characterized by the presence of elliptical voids which are thought to have formed as a result of a

velocity component perpendicular to the shear surface [25] or in an effort to reduce surface energy while under tensile forces [26]. Figure 12b shows further development of void growth in the shear bands leading to failure.

Porous Sandwich Builds

SHPB testing was performed on the porous sandwiches made from varying build parameters (Fig. 2) with the cores having porosities ranging from 2 to 45% (Fig. 6). Porosity was found to have a profound effect on the high strain rate response, as seen from the significant drop in the load required for displacement. Figure 13a shows the load–displacement curves of two specimens from each of the settings A–F. At each setting, the response of the two samples were very alike demonstrating good repeatability. The deformation was concentrated completely in the core while the face plates remained undeformed. Hence, the core dimensions were used in conversion of the load–displacement data into stress–strain data in order to compare the relative strength of the porous sandwiches with the fully dense builds from standard settings. These dynamic flow stresses are plotted in Fig. 13b.

In metallic foams, a mechanical property (P) can be given by a generic scaling law [27]:

$$\frac{P}{P_s} = \alpha \left(\frac{\rho}{\rho_s} \right)^n$$

where P is a property, P_s is the property of the solid, ρ is the density of the foam, ρ_s is the density of the solid material. The relative density of the foam is:

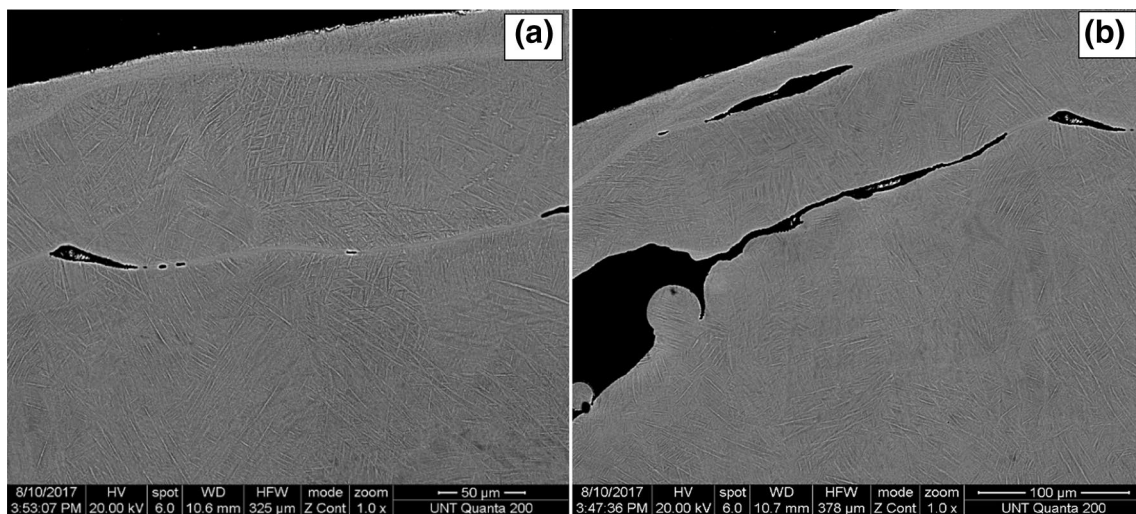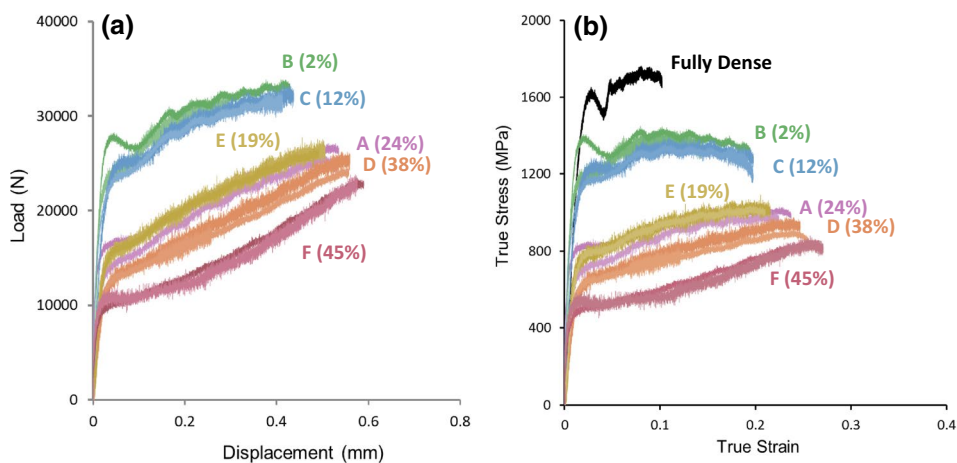$$\frac{\rho}{\rho_s} = 1 - \text{porosity}$$

Fig. 12 Fracture surface of 45° builds in stress relieved condition: **a** shows narrow shear band connecting elliptical shaped pores, **b** shows void growth in shear bands

Fig. 13 **a** Load and displacement curves of the porous sandwiches of settings *A–F*. **b** Dynamic flow stresses of the porous sandwiches compared to the fully dense as-built condition vertical build's response. Two specimens were tested for each of the settings and they showed repeatable response

The flow stresses of the porous sandwiches, a representative of their dynamic compressive strength, showed a good fit with this metallic foam model:

$$\frac{\sigma_{sandwich}}{\sigma_{as\text{-}built}} = \alpha\,(1 - porosity)^n$$

with constant $\alpha = 0.98$ and the exponent $n = 1.65$, and the fully dense material showing a flow stress of $\sigma_{as\text{-}built} = 1650$ MPa (Fig. 14a). This structural nature of response is also supported by the apparent increase in the flow stresses with strain in Fig. 13b at high levels of porosity. As Ti–6Al–4V shows very weak work hardening in the dynamic regime, this is clearly a manifestation of compacting/densification.

The as-built fully dense builds, while very strong with flow stresses on the order of 1650 MPa, had often failed by shear at compressive strains of ~ 9%. Therefore the total energy absorption per unit volume of the material, the area under the stress–strain curve, was moderate at ~ 150 J cm^{-3}. The porous sandwiches, while having lower strength, did not fail even at 20% strain and as a result had larger energy absorption. The sandwich with lowest porosity of 2%, setting B, had the highest energy absorption of 280 J cm^{-3}, almost twice as much as the as-built, fully dense material. Further increases in porosity resulted in a steady decrease in their energy absorption (Fig. 14b) due to dropping flow stresses. Therefore with small amounts of porosity early shear failures were prevented, without a significant loss in strength, leading to very high energy absorption capacity.
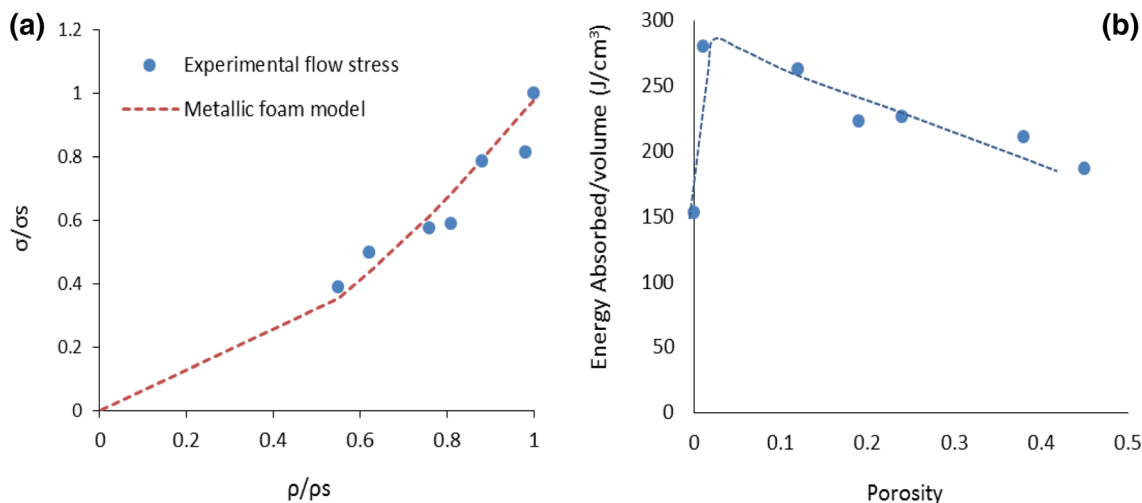
Fig. 14 **a** Dynamic flow stresses showing a good fit with the scaling law for metallic foams, **b** energy absorption per unit volume as a function of porosity shows the 2% porous sandwich to have the highest capacity owing to the high flow stresses and greater resistance to failure

Conclusions

A comprehensive investigation of the dynamic mechanical properties of additively built Ti–6Al–4V alloy has been performed. The effect of orientation, location on build plate, and post-build heat treatments have been studied simultaneously through a set of specimens of 45 different initial conditions. The dynamic flow stress data from testing these specimens using SHPB offers several interesting insights:

1. The as-built and stress-relieved microstructures looked alike and had heterogeneous microstructures composed of 50–100 μm wide columnar prior-β grains that consisted of acicular α′ needles. This martensitic structure gave rise to very high dynamic strength of over 1600 MPa.
2. The as-built material had significant internal stresses which varied across the location on the build plate resulting in a scattered data set.
3. Stress-relief treatment brought more locationally homogeneous response, but the retained microstructural anisotropy caused the 45° builds to have slightly higher strength with a greater propensity for catastrophic failure by formation of adiabatic shear bands.
4. HIP treatment at a post β-transus temperature converted the martensite to a bimodal α/β microstructure. The high temperature and long duration also resulted in modification of the prior-β grain structure eliminating the anisotropy. The bimodal structure that formed from partial dynamic globularization due to application of stress during the cool down resulted in greater ductility but a lower dynamic strength of about 1400 MPa.
5. HIP appeared to be a necessary heat treatment to achieve a complete uniform response that is independent of both the location and orientation of the build.
6. The study on porous sandwiches showed that induced porosity could be controlled by variation of the following build parameters: scan speed, laser power, and hatch spacing. Induced porosity was found to have a significant influence on the flow stresses, which could be well described by metallic foam scaling laws. Presence of a small porosity prevented shear failure at small strains, but without substantial strength loss, resulting in very high energy absorption capacity.

References

1. Vilaro T (2011) As-fabricated and heat-treated microstructures of the Ti-6Al-4V alloy processed by selective laser melting. Metall Mater Trans A 42(10):3190–3199
2. Baufeld B (2011) Wire based additive layer manufacturing: comparison of microstructure and mechanical properties of Ti-6Al-4V components fabricated by laser-beam deposition and shaped metal deposition. J Mater Process Technol 211:1146–1158
3. Vrancken B (2012) Heat treatment of Ti6Al4V produced by selective laser melting: microstructure and mechanical properties. J Alloys Compd 541:177–185
4. Carroll BE (2015) Anisotropic tensile behavior of Ti–6Al–4V components fabricated with directed energy deposition additive manufacturing. Acta Mater 87:309–320
5. Wauthle R (2015) Effects of build orientation and heat treatment on the microstructure and mechanical properties of selective laser melted Ti6Al4V lattice structures. Addit Manuf 5:77–84
6. Palanivel S (2016) Spatially dependent properties in a laser additive manufactured Ti-6Al-4V component. Mater Sci Eng A 654:39–52
7. Lee W (1998) Plastic deformation and fracture behaviour of Ti–6Al–4V alloy loaded with high strain rate under various temperatures. Mater Sci Eng A 241(1):48–59
8. Biswas N (2012) Deformation and fracture behavior of laser processed dense and porous Ti6Al4V alloy under static and dynamic loading. Mater Sci Eng A 549:213–221
9. Valdez M (2017) Induced porosity in super alloy 718 through the laser additive manufacturing process: microstructure and mechanical properties. J Alloys Compd 725:757–764
10. Pattanayak D (2011) Fabrication of bioactive porous Ti metal with structure similar to human cancellous bone by selective laser melting. Bioceram Dev Appl. https://doi.org/10.4303/bda/D101206
11. Chen WW (2010) Split Hopkinson (Kolsky) bar: design, testing and applications. Springer, New York
12. Ahmed T (1998) Phase transformations during cooling in α + β titanium alloys. Mater Sci Eng A 243(1):206–211
13. Semiatin SL (1999) Flow behavior and globularization kinetics during hot working of Ti–6Al–4V with a colony alpha microstructure. Mater Sci Eng A 263(2):257–271
14. Lee D (2004) Dynamic deformation behavior and ballistic impact properties of Ti-6Al-4V alloy having equiaxed and bimodal microstructures. Metall Mater Trans A 35(10):3103–3112
15. Zuo JH (2008) Effect of microstructure on ultra-high cycle fatigue behavior of Ti–6Al–4V. Mater Sci Eng A 473(1):147–152
16. Lu SL (2015) Microstructure and mechanical properties of long Ti-6Al-4V rods additively manufactured by selective electron beam melting out of a deep powder bed and the effect of subsequent hot isostatic pressing. Metall Mater Trans A 46(9):3824–3834
17. Gangireddy S (2017) High temperature dynamic response of a Ti-6Al-4V alloy: a modified constitutive model for gradual phase transformation. J Dyn Behav Mater 3(4):557–574
18. Nemat-Nasser S, Guo WG, Nesterenko VF, Indrakanti SS, Gu YB (2001) Dynamic response of conventional and hot isostatically pressed Ti–6Al–4V alloys: experiments and modeling. Mech Mater 33(8):425–439
19. Gray III GT, Livescu V, Rigg PA, Trujillo CP, Cady CM, Chen SR, Carpenter JS, Lienert TJ, Fensin SJ (2017) Structure/property (constitutive and spallation response) of additively manufactured 316L stainless steel. Acta Mater 138:140–149
20. Al-Bermani SS (2010) The origin of microstructural diversity, texture, and mechanical properties in electron beam melted Ti-6Al-4V. Metall Mater Trans A 41(13):3422–3434

21. Seo S (2005) Constitutive equation for Ti–6Al–4V at high temperatures measured using the SHPB technique. Int J Impact Eng 31(6):735–754
22. Jones DR, Fensin SJ, Dippo O, Beal RA, Livescu V, Martinez DT, Trujillo CP, Florando JN, Kumar M, Gray GT III (2016) Spall fracture in additive manufactured Ti-6Al-4V. J Appl Phys 120(13):135902
23. Timothy SP (1987) The structure of adiabatic shear bands in metals: a critical review. Acta Metall 35(2):301–306
24. Timothy SP (1985) The structure of adiabatic shear bands in a titanium alloy. Acta Metall 33(4):667–676
25. Rogers H (1974) Adiabatic shearing: a review. USA Army Research Office, Drexel University, Philadelphia, PA
26. Dormeval R (1987) The adiabatic shear phenomenon. Elsevier, London
27. Ashby MF (2000) Metal foams: a design guide, Chap. 4. Elsevier, London, pp 53–55